The Astrophysical Journal Letters, 735:L9 (7pp), 2011 July 1 doi:10.1088/2041-8205/735/1/L9

LAGRANGIAN COHERENT STRUCTURES IN NONLINEAR DYNAMOS

E. L. Rempel[1,2], A. C.-L. Chian[1,3,4], and A. Brandenburg[5,6]
[1] Institute of Aeronautical Technology (ITA), World Institute for Space Environment Research (WISER), São José dos Campos, SP 12228-900, Brazil; rempel@ita.br, abraham.chian@gmail.com
[2] Department of Applied Mathematics and Theoretical Physics (DAMTP), University of Cambridge, Cambridge CB3 0WA, UK
[3] National Institute for Space Research (INPE), World Institute for Space Environment Research (WISER), P.O. Box 515, São José dos Campos, SP 12227-010, Brazil
[4] California Institute of Technology, Pasadena, CA 91125, USA
[5] NORDITA, AlbaNova University Ctr, Stockholm, Sweden; brandenb@nordita.org
[6] Department of Astronomy, Stockholm University, SE-10691 Stockholm, Sweden
Received 2010 November 23; accepted 2011 May 2; published 2011 June 6

ABSTRACT

Turbulence and chaos play a fundamental role in stellar convective zones through the transport of particles, energy, and momentum, and in fast dynamos, through the stretching, twisting, and folding of magnetic flux tubes. A particularly revealing way to describe turbulent motions is through the analysis of Lagrangian coherent structures (LCSs), which are material lines or surfaces that act as transport barriers in the fluid. We report the detection of LCSs in helical MHD dynamo simulations with scale separation. In an Arnold–Beltrami–Childress flow, two dynamo regimes, a propagating coherent mean-field regime and an intermittent regime, are identified as the magnetic diffusivity is varied. The sharp contrast between the chaotic tangle of attracting and repelling LCSs in both regimes permits a unique analysis of the impact of the magnetic field on the velocity field. In a second example, LCSs reveal the link between the level of chaotic mixing of the velocity field and the saturation of a large-scale dynamo when the magnetic field exceeds the equipartition value.

Key words: chaos – dynamo – magnetohydrodynamics (MHD)

Online-only material: color figures

1. INTRODUCTION

The equipartition-strength magnetic fields observed in planets and stars are the result of a dynamo process, whereby kinetic energy from the motion of a conducting fluid is converted into magnetic energy (Brandenburg & Subramanian 2005). Initially, a weak seed magnetic field $\boldsymbol{B}$ undergoes a linear growth in the so-called kinematic dynamo phase until $\boldsymbol{B}$ is strong enough to impact the fluid velocity $\boldsymbol{u}$. Eventually, the magnetic energy saturates due to nonlinear effects. In a fast dynamo, the growth rate is positive and non-vanishing even in the limit where the magnetic Reynolds number tends to infinity. It is known that the growth of the magnetic energy in fast dynamos is related to the presence of Lagrangian chaos in the velocity field, i.e., scalar quantities passively advected by the flow (passive scalars) exhibit chaotic motions (Childress & Gilbert 1995; Balsara & Kim 2005). As $\boldsymbol{B}$ grows, it may suppress this chaos due to backreaction in the velocity field via the Lorentz force, leading to the nonlinear saturation of the magnetic energy (Cattaneo et al. 1996; Zienicke et al. 1998). A comparison between the chaoticity of the velocity field during the growth and saturation phases of the dynamo was performed by Brandenburg et al. (1995). In this Letter, we reveal how magnetic fields can affect the transport of passive scalars through the formation of transport barriers in the velocity field.

When probing turbulent transport of passive scalars, either Eulerian or Lagrangian tools can be employed. In the Eulerian approach, for a given velocity field, one can solve an advection–diffusion equation for the passive scalar concentration from which a turbulent diffusion coefficient can be computed (Vincent et al. 1996). Moreover, instantaneous snapshots of tracer and velocity fields can be used to extract coherent structures such as eddies and filaments (Isern-Fontanet et al. 2004). Alternatively, in the Lagrangian approach the dynamics of fluids is studied by following the trajectories of a large number of fluid elements or tracer particles. The Lagrangian description has been gaining increasing attention in the past decade, for example, in the study of compressible plasmas (Schamel 2004; Padberg et al. 2007). It has been suggested that Lagrangian tools are more appropriate to analyze tracer patterns than their Eulerian counterparts, since they do not rely solely on snapshots of the velocity field, but measure transport properties along particle trajectories (d'Ovidio et al. 2009). We adopt the Lagrangian approach to distinguish the transport properties of three-dimensional (3D) numerical simulations of compressible magnetohydrodynamic (MHD) dynamos. We detect Lagrangian coherent structures (LCSs), which are material lines and surfaces in the velocity field that act as barriers to particle transport and have been described as the Lagrangian building blocks of turbulence (Mathur et al. 2007). There are two types of LCSs formed by distinct groups of fluid particles, one of them attracts other fluid particles and the other one repels them. These barriers have been used to study turbulence and transport in fluids and plasmas through numerical simulations (Green et al. 2007; Padberg et al. 2007), laboratory experiments (Voth et al. 2002; Mathur et al. 2007), and observational data in oceans and a wide range of applications (Sandulescu et al. 2007; Olascoaga et al. 2008; Peacock & Dabiri 2010).

Two dynamo models with helical forcing and scale separation are used, the Arnold–Beltrami–Childress (ABC) flow (Childress & Gilbert 1995) and an isotropic flow driven by a force corresponding to plane waves with random phases (Brandenburg 2001). In the ABC flow, two different dynamo regimes are investigated, a regime characterized by a robust spatially coherent mean field and a regime with intermittent switching between coherent and disordered mean-field states.

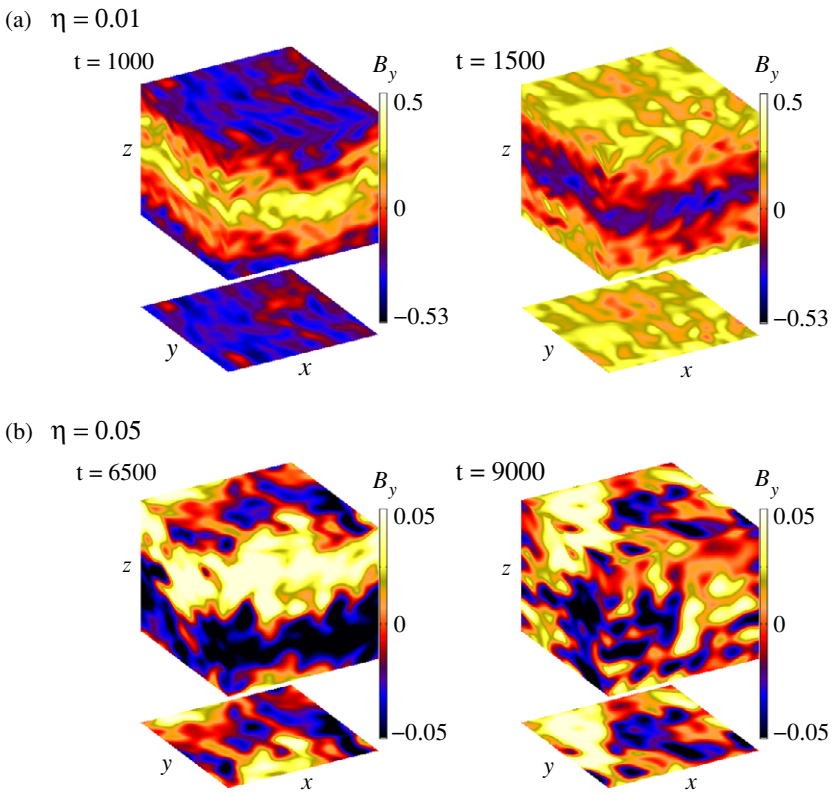

Figure 1. Intensity plots of B_y. (a) The propagation of a large-scale coherent pattern along the z-direction for $\eta = 0.01$. (b) Switching between ordered ($t = 6500$) and disordered ($t = 9000$) patterns for $\eta = 0.05$.

(A color version of this figure is available in the online journal.)

Here, the LCSs reveal that the topology of transport barriers in the velocity field suffers a dramatic change when the magnetic field undergoes the transition from coherent to intermittent dynamo. In the second dynamo model, the randomly forced flow, we focus on the problem of the nonlinear saturation of the magnetic energy. We note a large difference between the patterns of transport barriers in the kinematic and saturated regimes.

An ultimate goal of this project is to interrelate results from the Eulerian and Lagrangian approaches. For example, within the Eulerian approach it has been possible to compute mean-field dynamo transport coefficients and their magnetic quenching behavior using the test-field method (Brandenburg et al. 2008). The quenching is being interpreted in terms of a competition between kinetic helicity that results in an α effect and current helicity that produces a magnetic α effect. In an inhomogeneous system, the local current helicity distribution results from a balance accomplished by magnetic helicity fluxes (see Brandenburg & Subramanian 2005 for a review). If there is a direct connection between LCSs and the suppression of turbulent transport and, in particular, the α effect, one might expect a certain correlation in the spatial patterns of these quantities. As a preparatory first step, we establish here the basic technique in the case of a homogeneous turbulent dynamo.

2. INTERMITTENT DYNAMO IN THE ABC FLOW

The dynamo model adopted consists of the compressible MHD equations for an isothermal fluid, as described by Rempel et al. (2009b). The equations are solved with the PENCIL CODE[7] in a box with sides $L = 2\pi$ and periodic boundary conditions, so the smallest wavenumber is $k_1 = 1$. The sound speed is $c_s = 1$, so our time unit is $(c_s k_1)^{-1}$ and the unit of viscosity ν and magnetic diffusivity η is c_s/k_1. We add to the momentum equation an external forcing given by the ABC function, $\boldsymbol{f}(\boldsymbol{x}) = A_f/\sqrt{3}[(\sin k_f z + \cos k_f y)\hat{\boldsymbol{x}}, (\sin k_f x + \cos k_f z)\hat{\boldsymbol{y}}, (\sin k_f y + \cos k_f x)\hat{\boldsymbol{z}}]$, where A_f is the amplitude and k_f is the wavenumber of the forcing function. We use $k_f = 5$ to obtain a separation between the energy injection scale and the scale of the box, and $A_f = 0.1$, which ensures a root-mean-square velocity $u_{\rm rms} = \langle \boldsymbol{u}^2 \rangle^{1/2} < 0.4$. Following Rempel et al. (2009b), a numerical resolution of 64^3 mesh points is chosen. The kinetic (Re) and magnetic (Rm) Reynolds numbers are based on the forcing scale, $Re = u_{\rm rms}/\nu k_f$ and $Rm = u_{\rm rms}/\eta k_f$, where ν is the average kinematic viscosity and η is the constant magnetic diffusivity.

We fix $\nu = 0.005$, which in the absence of magnetic fields corresponds to a weakly turbulent flow with $Re \approx 16$. For large values of η, the seed magnetic field decays rapidly and there is no dynamo. After the onset of dynamo action at $\eta \approx 0.053$ ($Rm \approx 1.5$), the magnetic energy starts to grow at the expense of kinetic energy, until it saturates. Examples of magnetic structures are depicted in Figure 1 for two values of η and different times. For $\eta = 0.01$ (Figure 1(a)), there is a coherent large-scale B_y component that propagates along the z-direction. For $\eta = 0.05$ (Figure 1(b)), the magnetic field displays an intermittent switching between ordered ($t = 6500$) and disordered ($t = 9000$) large-scale structures. The scale bars reveal that B_y at $\eta = 0.01$ is one order of magnitude stronger than at $\eta = 0.05$.

A better understanding of the spatiotemporal dynamics can be obtained by computing $\bar{B}_y$, the xy-averages of $\boldsymbol{B}$. The upper

[7] http://pencil-code.googlecode.com/

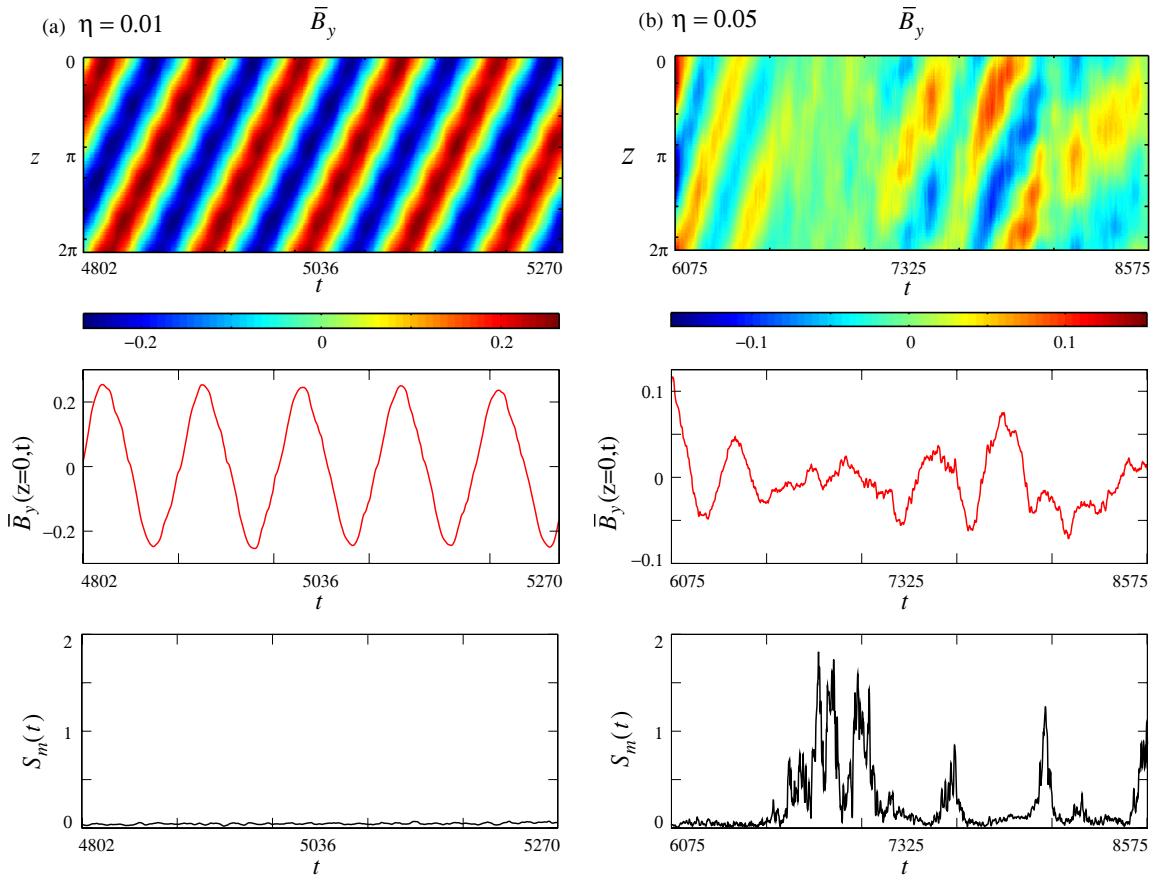

Figure 2. (a) Spacetime evolution of $\bar{B}_y$ (upper panel), the time series of $\bar{B}_y$ at $z = 0$ (mid panel), and the spectral entropy $S_m(t)$ (lower panel) for $\eta = 0.01$. (b) Same as (a) but for $\eta = 0.05$, displaying an intermittent dynamo.

(A color version of this figure is available in the online journal.)

panel in Figure 2 shows the spacetime evolution of $\bar{B}_y$ and the mid panel shows the time series of $\bar{B}_y$ at the point $z = 0$. The lower panel shows the spectral entropy $S_m(t)$, which is a measure of spatial complexity computed from the power spectra of $\bar{B}_y$ following Rempel et al. (2009a) and Chian et al. (2010). The left column refers to $\eta = 0.01$ and the right column to $\eta = 0.05$. The left column shows that the mean field for $\eta = 0.01$ propagates like a robust spatially coherent dynamo wave. The corresponding velocity field displays a mean flow with propagating oscillations. The direction of propagation is arbitrary and depends on the initial condition, which shows that there is multistability in the system. For $\eta = 0.05$ (right panel), the mean field is more fragile and there is on–off intermittency, with phases of spatially disordered patterns interspersed with phases of spatially coherent structures. We call the regime at $\eta = 0.01$ "dynamo wave" and at $\eta = 0.05$ "intermittent dynamo." The time-averaged values of the spectral entropy are $\langle S_m(t)\rangle_t \approx 0.045$ for $\eta = 0.01$ and $\langle S_m(t)\rangle_t \approx 0.33$ for $\eta = 0.05$.

The effect of the magnetic field on the velocity field and its transport properties can be studied using the maximum finite-time Lyapunov exponent (FTLE). The maximum FTLE, $\sigma_1^{t_0+\tau}(\boldsymbol{x})$, gives the finite-time average of the maximum rate of divergence or stretching between the trajectories of a fiducial particle at $\boldsymbol{x}(t)$ and its neighboring particles from time $t = t_0$ to $t = t_0 + \tau$ (Shadden et al. 2005). A positive σ_1 is the signature of chaotic streamlines in the velocity field. FTLEs are able to detect LCSs, which are the time-dependent analogous of stable and unstable manifolds of invariant sets in time-independent velocity fields. For a 3D time-dependent velocity field, regions of maximum material stretching generate local maximizing curves (*ridges*) in the FTLE field. Thus, repelling LCSs (finite-time stable manifolds) produce ridges in the maximum FTLE field in the forward-time dynamics and attracting LCSs (finite-time unstable manifolds) produce ridges in backward time (Haller 2001; Shadden et al. 2005; Padberg et al. 2007).

Since backward-time integration of dissipative systems is a major problem due to numerical instabilities (Celani et al. 2004), we have to resort to interpolation of recorded data. A run from $t_0 - \tau$ to $t_0 + \tau$ is conducted and full 3D snapshots of the velocity field are saved at each $dt = 0.5$ time interval. Linear interpolation in time and third-order Hermite interpolation in space are used to obtain the continuous vector fields necessary to obtain the particle trajectories. For backward time, the interpolated snapshots from t_0 to $t_0 - \tau$ are used and the particle trajectories are computed with a fourth-order Runge–Kutta method. The choice of the spatial interpolation scheme may affect the local dynamics of individual particles, which can result in minor changes in the delimitation of some of the material lines detected. Here, we adopted a third-order interpolation which is the standard scheme employed in the literature for computing FTLE (see Haller & Yuan 2000; Shadden et al. 2005; Padberg et al. 2007; Mathur et al. 2007; Mendoza & Mancho 2010). We compared the results obtained for the ABC flow with the known results from the literature and they show excellent agreement.

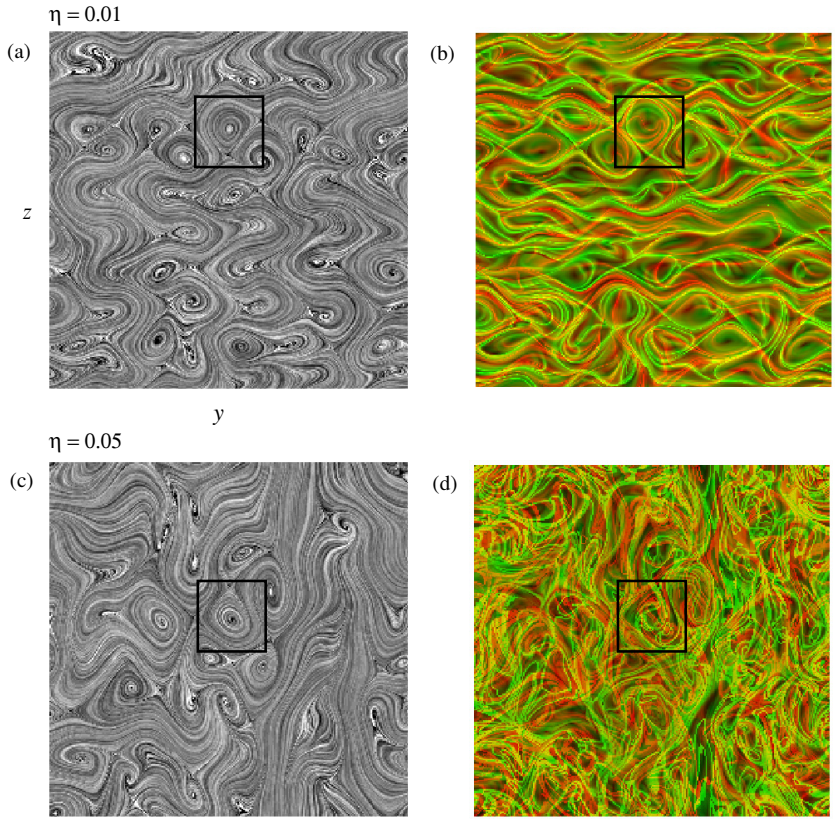

Figure 3. (a) Line integral convolution plot of the (y, z) components of a snapshot of the velocity field at $x = 0$ for the wave dynamo at $\eta = 0.01$. (b) The corresponding repelling (green) and attracting (red) LCSs represented by material lines. (c and d) Same as (a) and (b), but for the intermittent dynamo at $\eta = 0.05$.
(A color version of this figure is available in the online journal.)

Figure 3 illustrates the difference between the LCS of the wave and intermittent dynamos. Figure 3(a) shows a visualization of the (y, z) components of the velocity field for $\eta = 0.01$ at $x = 0$ using the technique of line integral convolution, which shows the integral curves of (u_y, u_z) in different tones of gray. This snapshot was computed for $t_0 = 2000$, when the magnetic energy of the dynamo wave has already saturated (see Figure 2(a)). The corresponding LCSs are shown in Figure 3(b), where green and red lines represent the repelling and attracting material lines, respectively. The LCSs represent the $\sigma_1^{t_0+\tau}$ field computed with $\tau = \pm 10$. Figure 3(b) is plotted as a three-vector RGB image using Octave's imshow routine, where the forward-time σ_1 field is stored in the "green vector" and the backward-time σ_1 field in the "red vector." Note that the intersections between high-intensity red and green lines may produce yellow points. We stress that the important feature of these plots is not the absolute value of σ_1, but the ridges in its field, so the color maps are normalized by the largest value of σ_1. Figures 3(c) and (d) plot the velocity field and LCS, respectively, for the intermittent regime at $\eta = 0.05$ ($t_0 = 2000$ and $\tau = \pm 10$). The LCS distinguish the dynamo wave and intermittent dynamo regimes quite well. This becomes clearer in Figure 4, which depicts enlargements of the rectangular regions in Figure 3. For the dynamo wave (Figures 4(a) and (b)), a large eddy in Figure 4(a) is seen in the LCS plot of Figure 4(b) as a "smooth" region with a low level of particle dispersion bordered by attracting and repelling material lines. The entanglement of attracting and repelling LCSs is responsible for the transport of particles between eddies (in two-dimensional flows this transport mechanism is called lobe dynamics; Rom-Kedar & Wiggins 1990). The X-point marked with an arrow in Figure 4(b) specifies the location of a hyperbolic trajectory nearby a point where the velocity field is instantaneously zero in the (y, z) projection (see the velocity field near the arrow in Figure 4(a)). The material lines are cross sections of material surfaces, and trajectories approach the X-point along the green line and are repelled from it along the red line. For the intermittent dynamo (Figures 4(c) and (d)), the entanglement is much more complex, even though the eddies in Figures 4(a) and (c) look similar. The Lagrangian plot unveils an intricacy of local structures which is not seen in the Eulerian frame. The arrows in Figures 4(c) and (d) mark the location of an X-point whose time-dependent manifolds, or LCS, fill the phase space in such a way that a border of the eddy cannot be identified. In the intermittent regime, the numerous crossings between attracting and repelling material lines enhance transport between regions. This transport can be quantified by the maximum FTLE $\sigma_1^{t_0+\tau}$ of the particle trajectories. The mean value for the dynamo wave at $\eta = 0.01$, obtained from a probability density function computed with the trajectories of 64^3 particles evenly distributed in the box, is $\sigma_1^{t_0+\tau} \approx 0.25$. For the intermittent dynamo at $\eta = 0.05$, $\sigma_1^{t_0+\tau} \approx 0.32$ and, therefore, the resulting chaotic mixing is more efficient. Although the LCSs vary according to t_0, in general the LCS fields computed at $\eta = 0.05$ display higher degree of complexity than at $\eta = 0.01$.

The enhancement in the flow's chaoticity when the magnetic diffusivity is increased from $\eta = 0.01$ to $\eta = 0.05$ is the result of a reduction of the effect of the Lorentz force upon the velocity field. For $\eta = 0.01$, $B_{\rm rms} \approx 0.27$ and $u_{\rm rms} \approx 0.29$, so the magnetic field can become strong enough to suppress Lagrangian chaos in the velocity field, inhibiting

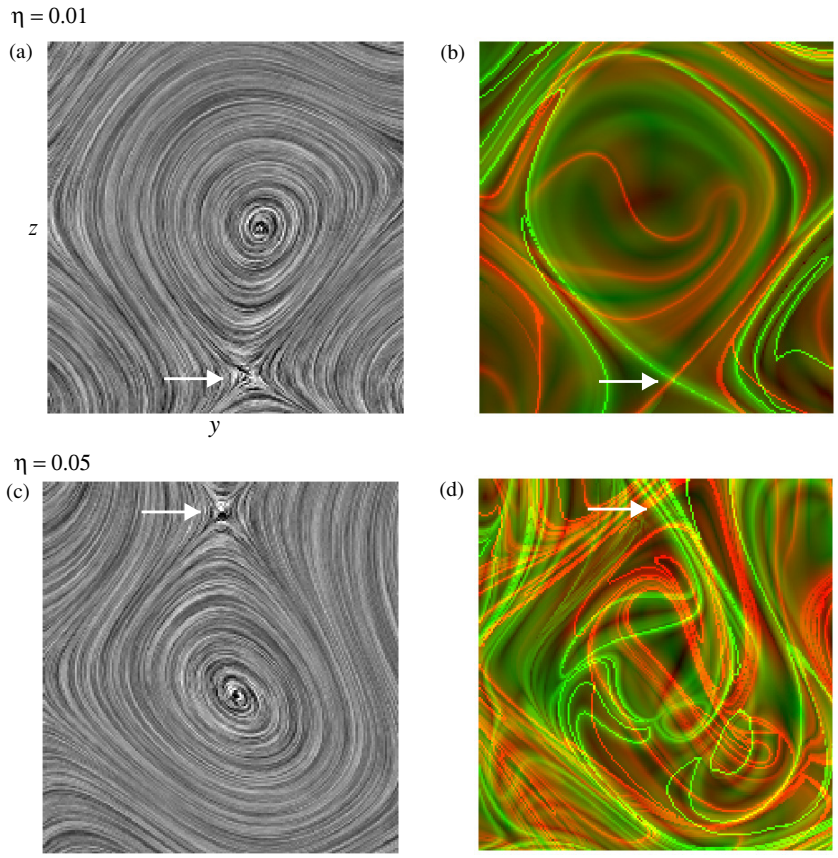

Figure 4. Enlargement of the rectangular areas in Figure 3. (a and b) The velocity field and Lagrangian coherent structures for $\eta = 0.01$. (c and d) Same as (a) and (b) but for $\eta = 0.05$.

(A color version of this figure is available in the online journal.)

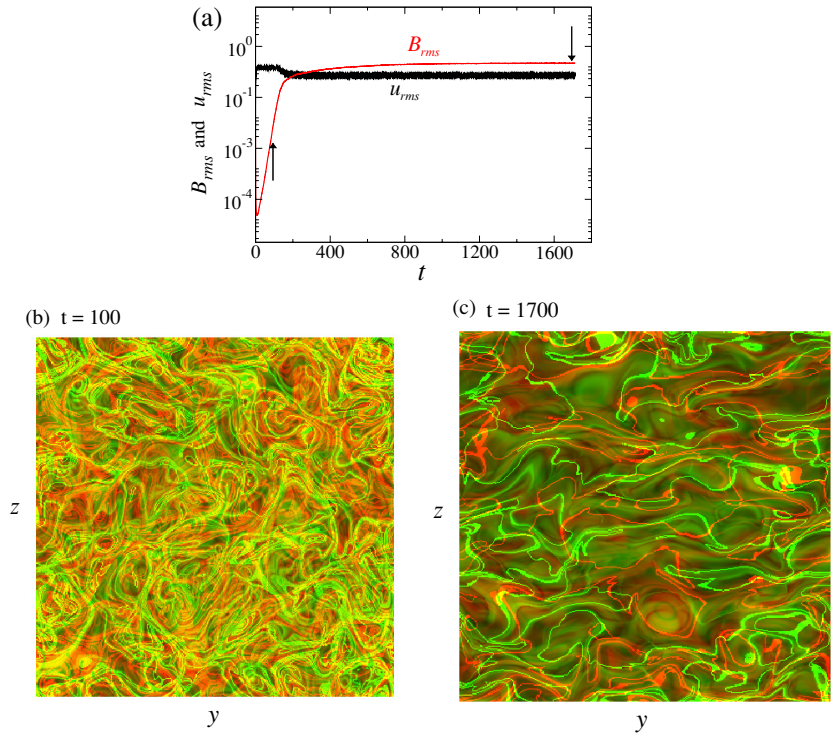

Figure 5. Turbulent simulations with random helical forcing. (a) Evolution of the total rms magnetic (red) and velocity (black) fields. The arrows point to $t = 100$ and $t = 1700$. (b) LCS for the kinematic dynamo at $t = 100$. (c) LCS for the saturated dynamo at $t = 1700$.

(A color version of this figure is available in the online journal.)

particle transport. As a result of lower chaoticity, as well as the backward transfer of magnetic energy from small to large scales due to kinetic helicity (α effect) present in this system, the magnetic field $\boldsymbol{B}$ saturates in an ordered state with the scale of the box and the mean-field dynamics resembles a spatially coherent propagating wave (Figure 2(a)). For $\eta = 0.05$, stronger magnetic diffusivity causes the magnetic field to be damped, with $B_{\rm rms} \approx 0.076$ and $u_{\rm rms} \approx 0.38$. A weaker magnetic field has small impact on the velocity field and Lagrangian chaos becomes stronger, with enhanced particle transport and chaotic mixing. The chaotic motions of the flow carry the magnetic field lines and generate the disordered $\boldsymbol{B}$ field states. On the other hand, stronger chaos in the velocity field leads to enhanced stretching, twisting, and folding of magnetic field lines, which tends to cause the magnetic energy to grow (Childress & Gilbert 1995). The growth of $\boldsymbol{B}$ backreacts on the velocity field, suppressing chaoticity again and leading to the intermittent occurrence of ordered $\boldsymbol{B}$ field patterns observed in the intermittent dynamo of Figures 1(b) and 2(b).

3. NONLINEAR DYNAMO SATURATION IN THE B2001 FLOW

For this section we have performed computations described in Brandenburg (2001; hereafter B2001), where the MHD equations are solved with a helical forcing with a time-dependent wavevector. At each time step, there is a random choice of wavevector with wavenumber k_f around 5. The resulting flow is essentially the prototype of the α^2 dynamo of mean-field dynamo theory. We have adopted run 3 of B2001, where $\nu = \eta = 0.002$ and the Reynolds number based on the box size is about 600 ($Re = Rm = 18$ as defined in Section 2 above) for a numerical resolution of 128^3. Due to an inverse cascade of magnetic helicity discussed in B2001, the magnetic field develops a robust spatially coherent mean-field pattern similar to the case $\eta = 0.01$ above (Figure 1(a)). Figure 5(a) shows the time evolution of $u_{\rm rms}$ and $B_{\rm rms}$ in log-linear scale, revealing the exponential growth of $B_{\rm rms}$ in the kinematic phase, before saturation. Figures 5(a) and (b) show the LCS computed for $\tau = \pm 10$ at $t_0 = 100$ (kinematic dynamo) and $t_0 = 1700$ (saturated nonlinear dynamo), respectively. In the kinematic regime the patterns of material lines in the LCS plot are highly complex, and the chaotic tangle permeates the phase space, which favors the growth of magnetic energy. In the nonlinear regime, since $B_{\rm rms}$ becomes considerably higher than $u_{\rm rms}$ (superequipartition), the chaoticity of the velocity field is strongly decreased due to the Lorentz force (Cattaneo et al. 1996; Zienicke et al. 1998). The crossings between the main attracting and repelling lines are scarce, so there is comparatively little dispersion of passive scalars and transport is inhibited. The level of chaotic mixing quantified by the average FTLE is $\sigma_1^{t_0+\tau} \approx 0.34$ for the kinematic dynamo and $\sigma_1^{t_0+\tau} \approx 0.18$ for the saturated dynamo.

4. CONCLUSIONS

We have shown that LCSs can be used for an in-depth exploration of particle transport in 3D MHD dynamo simulations. Our results agree with the previous results by Cattaneo et al. (1996) and Zienicke et al. (1998), who showed that the modification of the velocity field due to stronger $\boldsymbol{B}$ becomes clearer by examining the Lagrangian properties of the flow as measured by the FTLEs. Here, in addition to computing the forward-time FTLE field, the detection of attracting material lines as ridges in the backward-time FTLE field provides the pathways that are more likely to be followed by passive scalars in the fluid. Moreover, the superposed plots of both attracting and repelling LCSs permit the identification of the principal mixing zones of the fluid.

The two dynamo models adopted in this work exhibit weak turbulence, with reasonably low Reynolds numbers. Our goal was not to present state-of-the-art numerical simulations, but to introduce the LCS technique in the context of space/astrophysical plasmas using two important topics in the theory of nonlinear dynamos, namely, the onset of intermittency and the nonlinear saturation of the magnetic energy. Regarding the first topic, the connection between the Lorentz force and on–off dynamo intermittency in ABC flows was studied by Alexakis & Pontis (2008); on–off intermittency has also been observed in laboratory experiments with a dynamo generated by a flow of liquid sodium (Ravelet et al. 2008; Monchaux et al. 2009); besides, intermittent chaotic dynamos have been suggested as the cause of the long periods of low solar activity in the solar cycle, known as grand minima (Spiegel 2009). Concerning the second topic, it is one of the fundamental questions in dynamo theory and there is an extended list of papers that discuss the nonlinear saturation of $\boldsymbol{B}$ in dynamo simulations in periodic boxes with moderate Reynolds numbers (Brandenburg et al. 1995; Cattaneo et al. 1996; Zienicke et al. 1998; Brandenburg 2001; Brandenburg & Subramanian 2005; Käpylä & Brandenburg 2009; Cattaneo & Tobias 2009).

The LCS method can be readily employed in a number of problems related to the turbulent transport of passive scalars, including observational data, provided an estimation of the velocity vector field is available. Such estimations can be obtained from digital images using techniques such as the optical flow algorithm, employed by Colaninno & Vourlidas (2006) to extract the velocity field from images of coronal mass ejections obtained with the *Solar and Heliospheric Observatory* Large Angle and Spectromeric Coronagraph Experiment C2 coronagraph. Solar subsurface flows can also be inferred from helioseismic data (Woodard 2002), thus LCSs can aid the tracing of particle transport by turbulence in stellar interiors.

In conclusion, a proper understanding of Lagrangian chaotic mixing is crucial for understanding the dynamics of nonlinear dynamos as well as the elaboration of models of stellar interiors that can correctly account for the turbulent transport of particles, energy, and momentum in convective zones, and we believe that LCSs are an innovative tool that should be further explored in astrophysics.

E.L.R. thanks the University of Cambridge (DAMTP) for the hospitality and Professor Michael Proctor for valuable discussions. E.L.R. and A.C.L.C. acknowledge the support by CNPq (Brazil) and FAPESP (Brazil). A.C.L.C. acknowledges the award of a Guggenheim Fellowship and the hospitality of Caltech.

REFERENCES

Alexakis, A., & Pontis, Y. 2008, Phys. Rev. E, 77, 056308
Balsara, D. S., & Kim, J. 2005, ApJ, 634, 390
Brandenburg, A. 2001, ApJ, 550, 824
Brandenburg, A., Klapper, I., & Kurths, J. 1995, Phys. Rev. E, 52, R4602
Brandenburg, A., Rädler, K.-H., Rheinhardt, M., & Subramanian, K. 2008, ApJ, 687, L49
Brandenburg, A., & Subramanian, K. 2005, Phys. Rep., 417, 1
Cattaneo, F., Hughes, D. W., & Kim, E.-J. 1996, Phys. Rev. Lett., 76, 2057
Cattaneo, F., & Tobias, S. M. 2009, J. Fluid Mech., 621, 201
Celani, A., Cencini, M., & Noullez, A. 2004, Physica D, 195, 283

Chian, A. C.-L., Miranda, R. A., Rempel, E. L., Saiki, Y., & Yamada, M. 2010, Phys. Rev. Lett., 104, 254102
Childress, S., & Gilbert, A. D. 1995, Stretch, Twist, Fold: The Fast Dynamo (Berlin: Springer)
Colaninno, R. C., & Vourlidas, A. 2006, ApJ, 652, 1747
d'Ovidio, F., et al. 2009, Deep-Sea Res. I, 56, 15
Green, M. A., Rowley, C. W., & Haller, G. 2007, J. Fluid Mech., 572, 111
Haller, G. 2001, Physica D, 149, 248
Haller, G., & Yuan, G. 2000, Physica D, 147, 352
Isern-Fontanet, J., Font, J., García-Ladona, E., Emelianov, M., Millot, C., & Taupier-Letage, I. 2004, Deep-Sea Res. II, 51, 3009
Käpylä, P., & Brandenburg, A. 2009, ApJ, 699, 1059
Mathur, M., Haller, G., Peacock, T., Ruppert-Felsot, J. E., & Swinney, H. L. 2007, Phys. Rev. Lett., 98, 144502
Mendoza, C., & Mancho, A. N. 2010, Phys. Rev. Lett., 105, 038501
Monchaux, R., et al. 2009, Phys. Fluids, 21, 035108
Olascoaga, M. J., Beron-Vera, F. J., Brand, L. E., & Kocak, H. 2008, J. Geophys. Res., 113, C12014
Padberg, K., Hauff, T., Jenko, F., & Junge, O. 2007, New J. Phys., 9, 400
Peacock, T., & Dabiri, J. 2010, Chaos, 20, 017501
Ravelet, F., et al. 2008, Phys. Rev. Lett., 101, 074502
Rempel, E. L., Miranda, R. A., & Chian, A. C.-L. 2009a, Phys. Fluids, 21, 074105
Rempel, E. L., Proctor, M. R. E., & Chian, A. C.-L. 2009b, MNRAS, 400, 509
Rom-Kedar, V., & Wiggins, S. 1990, Arch. Ration. Mech. Anal., 109, 239
Sandulescu, M., Lopez, C., Hernández-García, E., & Feudel, U. 2007, Nonlinear Proc. Geophys., 14, 443
Schamel, H. 2004, Phys. Rep., 392, 279
Shadden, S. C., Lekien, F., & Marsden, J. E. 2005, Physica D, 212, 271
Spiegel, E. A. 2009, Space Sci. Rev., 144, 25
Vincent, A., Michaud, G., & Meneguzzi, M. 1996, Phys. Fluids, 8, 1312
Voth, G. A., Haller, G., & Gollub, J. P. 2002, Phys. Rev. Lett., 88, 254501
Woodard, M. F. 2002, ApJ, 565, 634
Zienicke, E., Politano, H., & Pouquet, A. 1998, Phys. Rev. Lett., 81, 4640